Check for updates

Analysis of the behavior of pulsed vortex beams in oceanic turbulence

H. Benzehoua[1] · A. Belafhal[1]

Abstract

This study aims to investigate the behavior of pulsed Laguerre higher-order cosh-Gaussian (LHChG) beam as they travel through turbulent oceanic environments. The propagation of the pulsed LHChG beam is analyzed using the extended Huygens-Fresnel principle and the Fourier Transform method. Additionally, the effects of ocean turbulence, transverse position, and initial beam parameters on the spectral intensity of the beam are examined numerically. The relative spectral shift of the pulsed LHChG beam in oceanic turbulence as a function of the transverse coordinate is also analyzed through numerical simulations and depicted graphically. Our results show that the spectral intensity of the beam depends on oceanic parameters such as the rate of dissipation of kinetic energy per unit mass of fluid, the dissipation rate of temperature variance, the ratio of temperature and salinity contributions to the refractive index spectrum and pulse duration. This research provides a physical explanation of the spectral transition of the pulsed LHChG beam propagating through the turbulent ocean. The findings of this study have potential applications in information coding and transmission.

1 Introduction

In recent decades, the propagation of laser beams through the turbulent environment has attracted more and more attention due to its important applications, such as laser communications, remote sensing, laser radar, laser weapons, and tracking. Many studies have been conducted to investigate the various properties of laser beams in turbulent medium, including beam wander (Wu et al. 2016), beam spreading (Chang et al. 2020), scintillation index (Korotkova et al. 2012; Boufalah et al. 2022), intensity distribution (Boufalah et al. 2018; Chib et al. 2020; Hricha et al. 2021; Nossir et al. 2021), field correlations of lasers, and more. At the same time, the field of ultrashort pulse

---

✉ A. Belafhal
belafhal@gmail.com

[1]   Laboratory LPNAMME, Laser Physics Group, Department of Physics, Faculty of Sciences, Chouaïb Doukkali University, P. B 20, 24000 El Jadida, Morocco

technology has made significant progress in recent years, attracting attention from numerous researchers and leading to a growing body of literature (Pan 2013; Zou and Hu 2016; Wang 2018; Duan et al. 2020; Li et al. 2020; Zhu et al. 2021; Benzehoua et al. 2021a, b; Liu and Lü 2004; Kandpal and Vaishy 2002). The investigation into how laser beams change spectrally, as they move through different media and optical systems, has gained significant attention. These advancements have opened up new possibilities in areas like optical communication, information encoding and transmission, and lattice spectroscopy (Yadav et al. 2007, 2008; Han 2009), with the potential for significant impact in the near future. Two types of spectral changes are observed: spectral shift and spectral switches. The first one refers to when the frequency of the spectrum shifts to either lower (red shift) or higher (blue shift) frequencies during the beam's propagation. Spectral switches is also a topic of interest in optical imaging systems and has been both theoretically predicted (Liu and Lü 2004) and experimentally verified (Kandpal and Vaishy 2002). Over the years, various studies have been conducted to explore the spectral changes of laser beams as they propagate through different media and optical systems. In 2016, Zou et al. investigated the spectral anomalies of a diffracted chirped pulsed super-Gaussian beam (Zou and Hu 2016). Duan et al. studied the impact of biological tissue and spatial correlation on the spectral changes of a Gaussian-Schell model vortex beam (Duan et al. 2020).

On the other hand, the propagation of laser beams in oceanic turbulence and the impact of factors such as salinity and temperature fluctuations on them has become a topics of increased interest. In recent times, the investigation of random beam propagation properties in oceanic turbulence has received considerable attention from researchers due to its practical applications in optical underwater communication, imaging, and sensing (Johnson et al. 2014). A number of studies have been conducted to investigate the evolution of various properties of stationary beams, such as intensity, coherence, polarization, beam quality, beam wander, beam scintillation, and spectral changes (Xu and Zhao 2014). Liu et al. studied the effect of oceanic turbulence on the spectral properties of a chirped Gaussian pulsed beam (Liu et al. 2016). Recently, Jo et al. studied the impact of oceanic turbulence on the spectral changes of a diffracted chirped Gaussian pulsed beam (Jo et al. 2022). This study aims to understand how oceanic turbulence affects the spectral characteristics of the beam as it diffracts, which can cause distortions in the beam's intensity and shape.

This paper focuses on examining the spectral characteristics of a pulsed LHChG beam when it travels through a turbulent oceanic environment. The pulsed LHChG beam is a versatile form of laser beam, which can also include pulsed Laguerre-Gaussian (LG) and Gaussian beams as special cases. Its intensity in the central region can be manipulated by changing the beam parameters, making it a useful tool for various applications. The cosh function used in the pulsed LHChG beam is a combination of Gaussian functions, additionally, the Laguerre-Gaussian beam, which is a Laguerre polynomial modulated by a Gaussian envelope, has already been demonstrated and has practical uses as a vortex beam. This work aims to analyze the spectral properties of pulsed LHChG beam propagation in turbulent oceanic environments. To the best of the authors' knowledge, this topic has not been previously studied. The structure of the current manuscript is as follows: In Sect. 2, we outline the electric field distribution of pulsed LHChG beam in cylindrical coordinates at the source plane and explain the theory model regarding the spectral characteristics of the considered pulsed beam during oceanic turbulence.

The influence of turbulent oceanic parameters and the beam on the evolution behavior of pulsed LHChG beam is presented in Sect. 3. In the end, the brief summary of the main results obtained is given in Sect. 4.

2 Propagation of pulsed LHChG through the oceanic turbulence

In order to analyze the propagation of pulsed LHChG beam in a turbulent oceanic environment, we first examine the propagation of its Fourier monochromatic component and then perform the inverse Fourier transform to determine the propagation equation in the space–time domain. The electric field distribution of the pulsed LHChG beam at source plane ($z = 0$) is defined in cylindrical coordinates

$$E_{l,m}^n(\rho, \phi, z = 0, t) = A_0 \left(\frac{\sqrt{2}}{w_0} \rho \right)^l L_m^l \left(\frac{2\rho^2}{w_0^2} \right) cosh^n \left(\Omega \rho^2 \right) \exp \left(-\frac{\rho^2}{w_0^2} \right) e^{il\phi} f(t), \quad (1)$$

where ρ and φ are radial and azimuthal coordinates, A_0 is a constant (to simplify, we will take it equal to 1), $L_m^l(.)$ denotes the Laguerre polynomial with m and l are the radial and angular mode orders, n is the order of the beam, w_0 is the waist width of the Gaussian part, $e^{il\phi}$ is the phase term for the beam, Ω is the displacement parameter associated with the cosh-part, and $f(t)$ is the temporal envelop of the initial pulsed beam with t is the time.

By using of the following relation between LG and Hermite-Gaussian modes (Abramowitz and Stegun 1970)

$$e^{il\phi} \rho^l L_m^l \left(\rho^2 \right) = \frac{(-1)^m}{2^{2m+l}m!} \sum_{p=0}^{m} \sum_{q=0}^{l} i^q \binom{m}{p} \binom{l}{q} H_{2p+l-q}(x) H_{2m-2p+q}(y), \quad (2)$$

where $H_j(.)$ is the jth order Hermite polynomial and $\binom{m}{p}$ denotes the binomial coefficient, and applying the following expression formula (Abramowitz and Stegun 1970)

$$\cosh^n \left(\rho^2 \right) = \frac{1}{2^n} \sum_{s=0}^{n} \frac{n!}{(n-s)!s!} e^{a_{sn}\rho^2}, \text{ with } a_{sn} = 2s - n \quad (3)$$

Equation (1) can be expressed in the following alternative form in Cartesian coordinates

$$E_{l,m}^n(x, y, z = 0, t) = \exp \left(-\frac{x^2}{w_{0x}^2} - \frac{y^2}{w_{0y}^2} \right) \sum_{p=0}^{m} \sum_{q=0}^{l} \frac{(-1)^m}{2^{2m+l+1}m!} i^q \binom{m}{p} \binom{l}{q} H_{2p+l-q} \left(\frac{\sqrt{2}x}{w_{0x}} \right) H_{2m-2p+q} \left(\frac{\sqrt{2}y}{w_{0y}} \right)$$

$$\times \frac{1}{2^n} \sum_{s=0}^{n} \frac{n!}{(n-s)!s!} \exp \left(\Omega a_{sn} x^2 \right) \exp \left(\Omega a_{sn} y^2 \right) f(t). \quad (4)$$

The last equation represents the input field for the pulsed LHChG beam, which is represented as a finite sum of Hermite–Gaussian modes in the x and y Cartesian coordinates with $r^2 = x^2 + y^2$.

Assume that the incident pulsed beam has a Gaussian form (Agrawal 1999)

$$f(t) = e^{-t^2/T^2} e^{-i\omega_0 t} \quad (5)$$

where T is the pulse duration and ω_0 is the central frequency.

Performing the Fourier transform on Eq. (4), we can obtain the following result, i.e., the field expressed in the space-frequency domain as

$$E(x, y, z = 0, \omega) = \frac{1}{\sqrt{2\pi}} \int\limits_{-\infty}^{+\infty} E(x, y, z = 0, t) e^{-i\omega t} dt = E(x, y, z = 0) f(\omega) \qquad (6)$$

where $f(\omega)$ is the original Fourier spectrum of the pulsed beam and is given by

$$f(\omega) = \frac{1}{\sqrt{2\pi}} \int\limits_{-\infty}^{+\infty} f(t) e^{i\omega t} dt \qquad (7)$$

On substituting from Eqs. (5) into (7), the integral calculation yields

$$S^{(0)}(\omega) = |f(\omega)|^2 = \left| \frac{T}{\sqrt{2}} \exp\left(\frac{-T^2(\omega - \omega_0)^2}{4} \right) \right|^2 \qquad (8)$$

where $S^{(0)}(\omega)$ is the original power spectrum of the incident beam.

The cross-spectral density function of pulsed LHChG beam at the input plane is given by

$$W_0(\mathbf{r_1}, \mathbf{r_2}, 0, \omega) = \left\langle E(x_1, y_1, 0, \omega) E^*(x_2, y_2, 0, \omega) \right\rangle, \qquad (9)$$

where $\mathbf{r_1} = (x_1, y_1)$ and $\mathbf{r_2} = (x_2, y_2)$ are two arbitrary position vectors in the source plane.

Being based on the extended Huygens-Fresnel principle (Andrews and Phillips 2005), the cross-spectral density function of pulsed LHChG beam propagating through the oceanic turbulence is expressed as

$$W_{l,m}^n(\boldsymbol{\rho_1}, \boldsymbol{\rho_2}, z, \omega) = \left(\frac{k}{2\pi z} \right)^2 S^{(0)}(\omega) \int\limits_{-\infty}^{+\infty} \int\limits_{-\infty}^{+\infty} W_0(\mathbf{r_1}, \mathbf{r_2}, 0) \exp\left[-\frac{ik}{2z}(\boldsymbol{\rho_1} - \mathbf{r_1})^2 + \frac{ik}{2z}(\boldsymbol{\rho_2} - \mathbf{r_2})^2 \right]$$
$$\times \left\langle \exp\left[\psi^*(\mathbf{r_1}, \boldsymbol{\rho_1}) + \psi(\mathbf{r_2}, \boldsymbol{\rho_2}) \right] \right\rangle_m d^2\mathbf{r_1} d^2\mathbf{r_2}, \qquad (10)$$

where $\boldsymbol{\rho_1}$ and $\boldsymbol{\rho_2}$ are two position vectors at the receiver plane. $k = \frac{\omega}{c}$ is the wave number with c is the speed of the source radiation in vacuum, $\langle . \rangle_m$ is the ensemble average over the statistics of the medium covering the fluctuation of log-amplitude and phase due to turbulent, $\psi(\mathbf{r}, \boldsymbol{\rho})$ denotes the random part of the complex phase, and the asterisk denotes complex conjugate. The expression for the ensemble average is obtained from the quadratic approximation of Rytov, given by (Andrews and Phillips 2005)

$$\left\langle \exp\left[\psi^*(\mathbf{r_1}, \boldsymbol{\rho_1}) + \psi(\mathbf{r_2}, \boldsymbol{\rho_2}) \right] \right\rangle_m \approx \exp\left\{ -\frac{1}{\rho_0^2} \left[(\mathbf{r_1} - \mathbf{r_2})^2 + (\mathbf{r_1} - \mathbf{r_2})(\boldsymbol{\rho_1} - \boldsymbol{\rho_2}) + (\boldsymbol{\rho_1} - \boldsymbol{\rho_2})^2 \right] \right\}. \qquad (11)$$

Thus, the spatial coherence radius of a spherical wave in oceanic turbulence is read as (Belafhal et al. 2021)

$$\rho_0 = \left[\frac{\pi^2}{3} k^2 z \int\limits_0^{+\infty} \kappa^3 \Phi_n(\kappa) d\kappa \right]^{-1/2}. \qquad (12)$$

In this paper, considering the finite outer scale of oceanic turbulence and eddy diffusivity ratio effects, the spatial power spectrum model of oceanic turbulence is expressed as (Li et al. 2019)

$$\Phi_n(\kappa) = \beta A^2 \varepsilon^{-\frac{1}{3}} \chi_t \frac{\left[1 + C_1(\kappa\eta)^{\frac{2}{3}}\right]}{4\pi\varpi^2\left(\kappa^2 + \kappa_0^2\right)^{\frac{11}{6}}} \left\{ \varpi^2 \exp\left[-\frac{(\kappa\eta)^2}{R_T^2}\right] + \frac{1}{d_r} \exp\left[-\frac{(\kappa\eta)^2}{R_S^2}\right] - \frac{1+d_r}{d_r}\varpi \exp\left[-\frac{(\kappa\eta)^2}{R_{TS}^2}\right] \right\},$$

(13)

where β is the Obukhov–Corrsin constant, $A = 2.6 \times 10^{-4}$ liter/deg, ε is the rate of dissipation of kinetic energy per unit mass of fluid ranging from 10^{-10} m^2/s^3 to 10^{-1} m^2/s^3, χ_t is the dissipation rate of temperature variance and has the range 10^{-10} K^2/s to 10^{-2} K^2/s, η is the inner scale of turbulence, κ is the spatial frequency of turbulent fluctuations ($0 < \kappa < \infty$), $\kappa_0 = 1/L_0$, L_0 is outer scale of turbulence, C_1 is a free parameter, ϖ is the ratio of temperature and salinity contributions to the refractive index spectrum, $R_i = \sqrt{3}\left[W_i - 1/3 + 1/(9W_i)\right]^{3/2}/Q^{3/2}$, $(i = T;S;TS)$ with $Q = 2.5$ is the non-dimensional constant, $W_i = \left\{ \left[\mathrm{Pr}_i^2/(6\beta Q^{-2})^2 - \mathrm{Pr}_i/(81\beta Q^{-2})\right]^{1/2} - \left[1/27 - \mathrm{Pr}_i/(6\beta Q^{-2})\right] \right\}^{1/3}$, $\mathrm{Pr}_T = 7$ and $\mathrm{Pr}_T = 700$ represent the Prandtl numbers of the temperature and salinity, respectively, $\mathrm{Pr}_{TS} = 2\,\mathrm{Pr}_T\,\mathrm{Pr}_S/(\mathrm{Pr}_T + \mathrm{Pr}_S)$, and d_r defines the eddy diffusivity ratio and can be expressed (Li et al. 2019)

$$d_r = \frac{|\varpi|}{R_F} \approx \begin{cases} 1/(1 - \sqrt{(|\varpi| - 1)/|\varpi|}) & |\varpi| \geq 1 \\ 1.85|\varpi| - 0.85 & 0.5 \leq |\varpi| \leq 1 \\ 0.15|\varpi| & |\varpi| \leq 0.5 \end{cases}$$

(14)

where R_F is the eddy flux ratio.

By invoking the integral formula (Belafhal et al. 2021).

$$\int_0^{+\infty} \frac{t^{2\mu-1}e^{-\varepsilon t^2}}{\left(1 + ct^2\right)^\nu}dt = \frac{\Gamma(\mu)}{2c^\mu}U\left(\mu;\mu+1-\nu;\frac{\varepsilon}{c}\right), \text{ with } \mu > 0\ \mu > 0$$

(15)

where $U(a;b;z)$ denoting the Tricomi function, and after tedious but straightforward integral calculations, the expression of the spatial coherence length can be arranged as

$$\rho_0 = \left(\frac{1}{24}\pi k^2 z\beta A^2 \varepsilon^{-\frac{1}{3}}\chi_t\right)^{-1/2} \left\{ \kappa_0^{1/3}\left[\begin{array}{c} U\left(2;\frac{7}{6};\frac{\kappa_0^2\eta^2}{R_T^2}\right) + \frac{1}{\varpi^2 d_r}U\left(2;\frac{7}{6};\frac{\kappa_0^2\eta^2}{R_S^2}\right) \\ -\frac{1+d_r}{\varpi d_r}U\left(2;\frac{7}{6};\frac{\kappa_0^2\eta^2}{R_{TS}^2}\right) \end{array} \right] + 1.191 C_1\eta^{\frac{2}{3}}\kappa_0 \times \left[\begin{array}{c} U\left(\frac{7}{3};\frac{3}{2};\frac{\kappa_0^2\eta^2}{R_T^2}\right) + \frac{1}{\varpi^2 d_r}U\left(\frac{7}{3};\frac{3}{2};\frac{\kappa_0^2\eta^2}{R_S^2}\right) \\ -\frac{1+d_r}{\varpi d_r}U\left(\frac{7}{3};\frac{3}{2};\frac{\kappa_0^2\eta^2}{R_{TS}^2}\right) \end{array} \right] \right\}^{-1/2}$$

(16)

In the next step, we will investigate the propagation properties of a pulsed LHChG beam through oceanic turbulence. By letting $\rho_1 = \rho_2 = \rho$ and inserting Eqs. (11) and (16) into Eq. (10), the following result is obtained

$$
\begin{aligned}
W_{l,m}^n(\rho,\rho,z,\omega) = {}& S^{(0)}(\omega)\left(\frac{k}{2\pi z}\right)^2 \frac{1}{2^{4m+2l+2n}(m!)^2} \sum_{p=0}^{m}\sum_{q=0}^{l}\sum_{r_1=0}^{m}\sum_{r_2=0}^{l}\sum_{s_1=0}^{n}\sum_{s_2=0}^{n}\binom{m}{p}\binom{l}{q}\binom{m}{r_1}\binom{l}{r_2}\binom{n}{s_1}\binom{n}{s_2} i^q(-i)^{r_2} \\
& \times \int\limits_{-\infty}^{+\infty}\int\limits_{-\infty}^{+\infty} H_{2p+l-q}\left(\sqrt{2}x_1\big/w_{0x}\right)\exp\left[-\beta_{1x}x_1^2 + 2\left(v_x + \frac{x_2}{\rho_0^2}\right)x_1\right]H_{2m-2p+q}\left(\sqrt{2}y_1\big/w_{0y}\right) \\
& \exp\left[-\beta_{1y}y_1^2 + 2\left(v_y + \frac{y_2}{\rho_0^2}\right)y_1\right]dx_1 dy_1 \times \int\limits_{-\infty}^{+\infty}\int\limits_{-\infty}^{+\infty} H_{2r_1+l-r_2}\left(\sqrt{2}x_2\big/w_{0x}\right) \\
& \exp\left[-\beta_{2x}x_2^2 - \frac{ik}{z}\rho_x x_2\right]H_{2m-2r_1+r_2}\left(\sqrt{2}y_2\big/w_{0y}\right)\exp\left[-\beta_{2y}y_2^2 - \frac{ik}{z}\rho_y y_2\right]dx_2 dy_2,
\end{aligned}
\tag{17}
$$

where

$$
\beta_{1j} = \frac{1}{w_{0j}^2} + \frac{1}{\rho_0^2} + \frac{ik}{2z} - \Omega a_{s_1 n},
\tag{18}
$$

$$
\beta_{2j} = \frac{1}{w_{0j}^2} + \frac{1}{\rho_0^2} - \frac{ik}{2z} - \Omega a_{s_2 n},
\tag{19}
$$

and

$$
v_j = \frac{ik\rho_j}{z},
\tag{20}
$$

with $(j = x$ or $y)$.

Furthermore, by using the expansion formulae (Abramowitz and Stegun 1970; Belafhal et al. 2020)

$$
H_n(x) = \sum_{k=0}^{[n/2]} (-1)^k \frac{n!}{k!(n-2k)!}(2x)^{n-2k},
\tag{21}
$$

$$
H_n(x+y) = \frac{1}{2^{n/2}} \sum_{k=0}^{n} \binom{n}{k} H_k\left(\sqrt{2}x\right)H_{n-k}\left(\sqrt{2}y\right),
\tag{22}
$$

and the following integrals

$$
\int\limits_{-\infty}^{+\infty} \exp\left(-px^2 + 2qx\right)H_m(\alpha x)\,dx = \sqrt{\frac{\pi}{p}}\exp\left(\frac{q^2}{p}\right)\left[1 - \frac{\alpha^2}{p}\right]^{m/2} H_m\left[\frac{\alpha q}{p\sqrt{1-(\alpha^2/p)}}\right],
\tag{23}
$$

and

$$
\int_{-\infty}^{+\infty} x^l \exp\left(-px^2 + 2qx\right) H_m(\alpha x)\, dx
$$

$$
= \sqrt{\frac{\pi}{p}} \frac{\exp\left(q^2/p\right)}{2^l} \sum_{k=0}^{[m/2]} \frac{(-1)^k m!}{k!(m-2k)!} H_{m+l-2k}\left(\frac{iq}{\sqrt{p}}\right) \left(\frac{\alpha}{i\sqrt{p}}\right)^{m+l-2k},
\tag{24}
$$

with $\Re e\, p > 0$, and after extensive algebraic calculations, the spectral intensity of a pulsed LHChG beam in oceanic turbulence is given by

$$
S_{l,m}^n\left(\rho_x, \rho_y, z, \omega\right) = W_{l,m}^n(\boldsymbol{\rho}, \boldsymbol{\rho}, z, \omega) = S^{(0)}(\omega) M_{l,m}^n\left(\rho_x, \rho_y, z, \omega\right)
\tag{25}
$$

where

$$
M_{l,m}^n\left(\rho_x, \rho_y, z, \omega\right) = \left(\frac{k}{2\pi z}\right)^2 \frac{1}{2^{5(m+0.5l)+2n}(m!)^2} \sum_{p=0}^m \sum_{q=0}^l \sum_{r_1=0}^m \sum_{r_2=0}^l \sum_{s_1=0}^n \sum_{s_2=0}^n
$$

$$
\binom{m}{p}\binom{l}{q}\binom{m}{r_1}\binom{l}{r_2}\binom{n}{s_1}\binom{n}{s_2} i^q(-i)^{r_2} S_x S_y,
\tag{26}
$$

with

$$
S_x = \frac{1}{\sqrt{\beta_{1x} b_x}} \exp\left(\frac{v_x^2}{\beta_{1x}} + \frac{\gamma_x^2}{b_x}\right) \left(1 - \frac{2}{w_{0x}^2 \beta_{1x}}\right)^{\frac{2p+l-q}{2}} \sum_{\mu=0}^{2p+l-q} \sum_{f_1=0}^{[\mu/2]} \sum_{h_1=0}^{[(2r_1+l-r_2)/2]} \binom{2p+l-q}{\mu}
$$

$$
\times \frac{(-1)^{f_1+h_1}}{2^{\mu-2f_1}} \frac{\mu!}{f_1!(\mu-2f_1)!} \frac{(2q+l-r_1)!}{h_1!(2r_1+l-r_2-2h_1)!} \left(\frac{2\sqrt{2}\alpha_x}{\rho_0^2}\right)^{\mu-2f_1}
$$

$$
\times \left(\frac{\sqrt{2}}{iw_{0x}\sqrt{b_x}}\right)^{2r_1+l-r_2+\mu-2f_1-2h_1} H_{2p+l-q-\mu}\left(\sqrt{2}\alpha_x v_x\right) H_{2r_1+l-r_2+\mu-2f_1-2h_1}\left(\frac{i\gamma_x}{\sqrt{b_x}}\right),
\tag{27}
$$

$$
S_y = \frac{1}{\sqrt{\beta_{1y} b_y}} \exp\left(\frac{v_y^2}{\beta_{1y}} + \frac{\gamma_y^2}{b_y}\right) \left(1 - \frac{2}{w_{0y}^2 \beta_{1y}}\right)^{\frac{2m-2p+q}{2}} \sum_{\sigma=0}^{2p+l-q} \sum_{f_2=0}^{[\sigma/2]} \sum_{h_2=0}^{[(2m-2r_1+r_2)/2]} \binom{2p+l-q}{\sigma}
$$

$$
\times \frac{(-1)^{f_2+h_2}}{2^{\sigma-2f_2}} \frac{\sigma!}{f_2!(\sigma-2f_2)!} \frac{(2m-2r_1+r_2)!}{h_2!(2m-2r_1+r_2-2h_2)!} \left(\frac{2\sqrt{2}\alpha_y}{\rho_0^2}\right)^{\sigma-2f_2}
$$

$$
\times \left(\frac{\sqrt{2}}{iw_{0y}\sqrt{b_y}}\right)^{2m-2r_1+r_2+\sigma-2f_2-2h_2} H_{2m-2p+q-\sigma}\left(\sqrt{2}\alpha_y v_y\right) H_{2m-2p+q+\sigma-2f_2-2h_2}\left(\frac{i\gamma_y}{\sqrt{b_y}}\right),
\tag{28}
$$

$$
b_j = \beta_{2j} - \frac{1}{\beta_j \rho_0^4},
\tag{29}
$$

$$
\gamma_j = v_j\left(\frac{1}{\beta_{1j}\rho_0^2} - 1\right),
\tag{30}
$$

and

$$\alpha_j = \frac{\sqrt{2}}{w_{0j}\beta_j\sqrt{1 - \left(2\big/ w_{0j}^2\beta_j\right)}}, \; (j = x \text{ or } y).$$ (31)

In Eq. (25), $M_{l,m}^n\left(\rho_x, \rho_y, z, \omega\right)$ is referred to as a spectral modifier. They state that the spectral intensity of this beam is determined by a combination of two factors: the original spectrum of the beam $S^{(0)}(\omega)$ and a spectral modifier $M_{l,m}^n\left(\rho_x, \rho_y, z, \omega\right)$. The original spectrum depends on the pulse duration T and the central frequency ω_0, while the spectral modifier depends on the observation point, propagation distance z, initial beam parameters and oceanic parameters.

Based on the findings from this Section, we will examine numerically the change in behavior of a pulsed LHChG beam as it travels through the turbulence in oceanic environment.

3 Simulation results and discussion

In this Section, the influence of oceanic turbulence on the spectral intensity of pulsed LHChG beam is demonstrated through numerical calculations using Eq. (25). The normalized on-axis and off-axis spectral intensities of the resulting beam after propagation through oceanic turbulence are discussed by using the relative spectral shift. This later is given by $\delta\omega\big/\omega_0 = \left(\omega_{\max} - \omega_0\right)\big/\omega_0$, where $\omega_{\max}$ is the frequency related to the maximum spectral intensity. For $\delta\omega\big/\omega_0 > 0$, the spectral intensity is blue-shifted and for $\delta\omega\big/\omega_0 < 0$, the spectral intensity is red-shifted. For the sake of simplicity, the normalized original spectrum is taken as $S^{00}(\omega) = S^{(0)}(\omega)/S^{(0)}\left(\omega_0\right)$, the normalized spectral intensity is $S_{l,m}^n(\omega) = S_{l,m}^n(\rho_x, \rho_y, z, \omega)/S_{l,m}^n(\rho_x, \rho_y, z, \omega_{\max})$ and the normalized spectral modifier is given by $M_{l,m}^n(\omega_0) = M_{l,m}^n(\rho_x, \rho_y, z, \omega_0)/M_{(l,m)\max}^n(\rho_x, \rho_y, z, \omega_0)$ where $M_{(l,m)\max}^n(\rho_x, \rho_y, z, \omega_0)$ is the maximum value of $M_{l,m}^n(\rho_x, \rho_y, z, \omega_0)$ at the observation point (ρ_x, ρ_y, z).
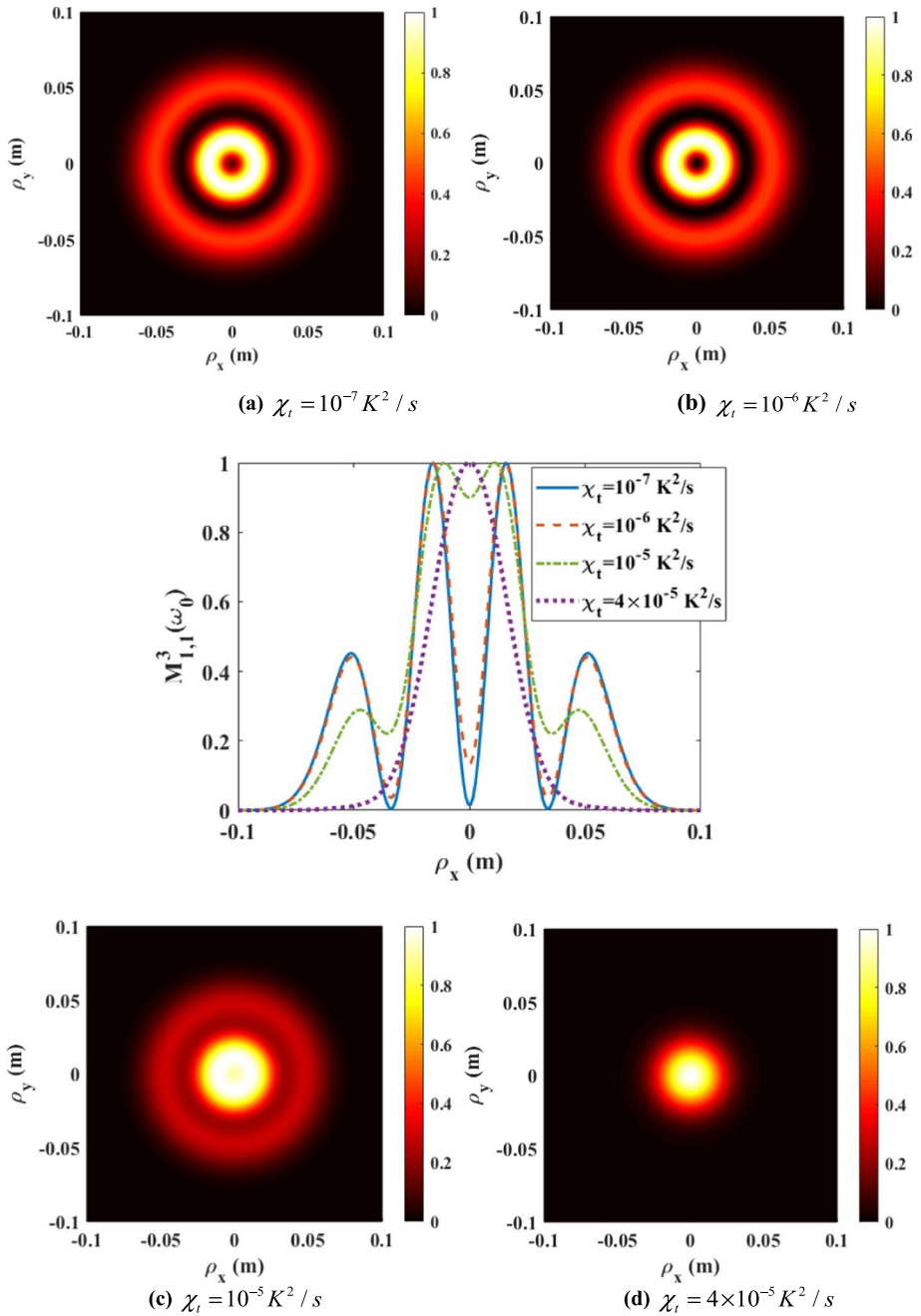
The study focuses on investigating the effects of oceanic turbulence on the spectral modifier of a pulsed LHChG beam during propagation. The calculation parameters are $\Omega = 0.1\,m^{-1}$, $\varepsilon = 10^{-7}\,m^2/s^3$, $\chi_t = 10^{-5}\,K^2/s, \varpi = -3$, $\lambda = 532\,nm$, $w_{0x} = w_{0y} = 1mm$, $\omega_0 = 2\pi c/\lambda$, m = l = 1 and $n=3$.

To begin this study, we depict in Fig. 1 the cross line ($\rho_y = 0$) and corresponding contour graphs of the normalized spectral modifier of a pulsed LHChG beam at the plane $z = 200\,m$ for several dissipation rates of temperature variance χ_t. As shown in Fig. 1, we observe that the pulsed LHChG beam will transform into a profile that resembles a Gaussian beam more quickly as the χ_t increases. This behavior can be attributed to the fact that the strength of oceanic turbulence intensifies with an increase in χ_t.
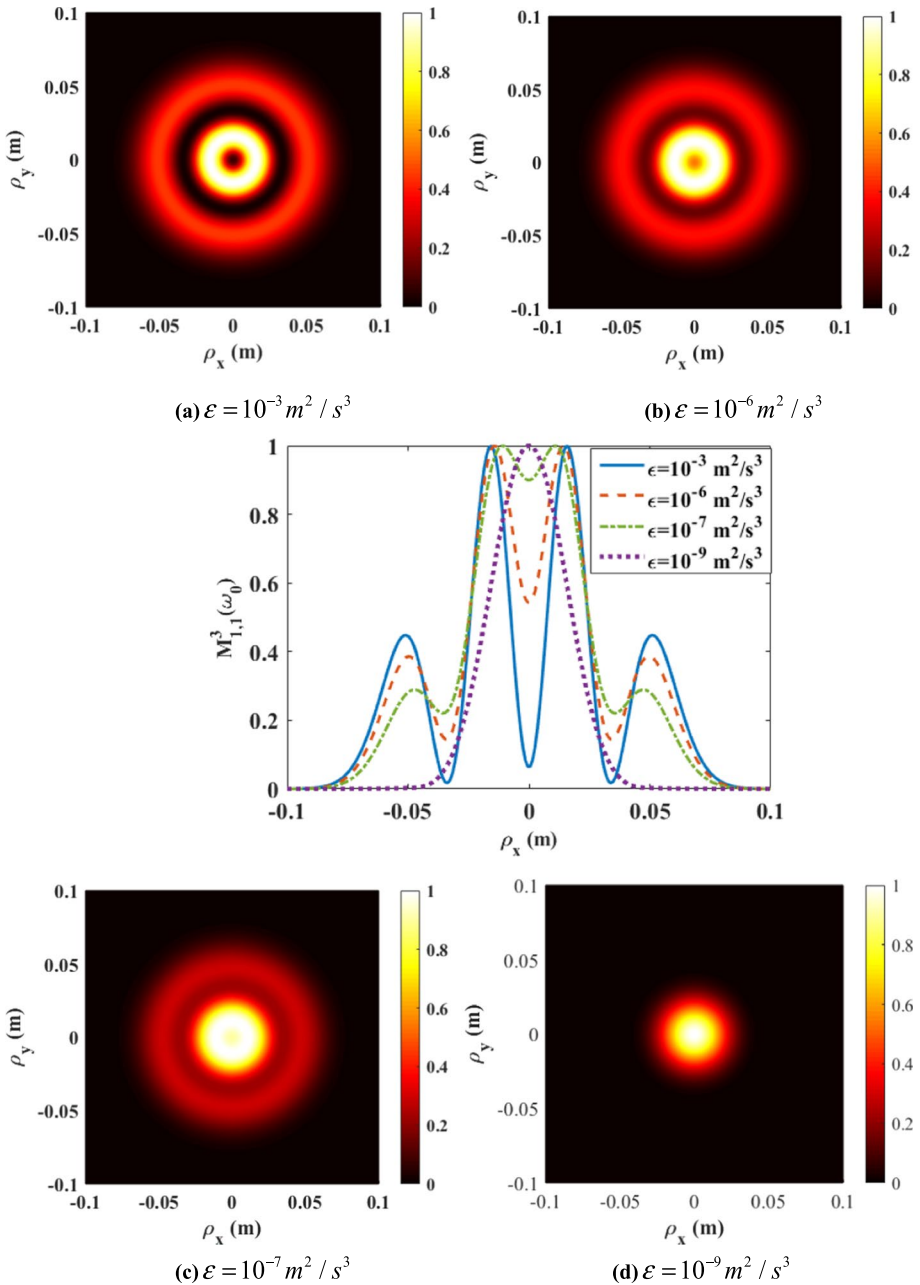
Figure 2 illustrates the cross line and contour graphs of the normalized spectral modifier of a pulsed LHChG beam for various rates of dissipation of kinetic energy per unit mass of fluid ε, using the calculation parameters outlined in Fig. 1.

The results indicate that as ε decreases, the pulsed LHChG beam transforms into a profile resembling a Gaussian beam more rapidly. This trend can be attributed to the fact that the strength of oceanic turbulence increases as ε decreases.

(a) $\chi_t = 10^{-7} K^2 / s$

(b) $\chi_t = 10^{-6} K^2 / s$

(c) $\chi_t = 10^{-5} K^2 / s$

**(d)** $\chi_t = 4 \times 10^{-5} K^2 / s$

Fig. 1 Evolution of the normalized spectral modifier of a pulsed LHChG beam in turbulence oceanic with several dissipation rates of temperature variance χ_t at a propagation distance $z = 200$ m

(a) $\varepsilon = 10^{-3} m^2 / s^3$

(b) $\varepsilon = 10^{-6} m^2 / s^3$

(c) $\varepsilon = 10^{-7} m^2 / s^3$

(d) $\varepsilon = 10^{-9} m^2 / s^3$

Fig. 2 Evolution of the normalized spectral modifier of a pulsed LHChG beam in turbulence oceanic with several rate of dissipation of kinetic energy per unit mass of fluid at a propagation distance $z = 200\,m$

Here, we present the impact of initial beam parameters, oceanic turbulence, and transverse positions on the spectral intensity and relative spectral shifts of the pulsed LHChG beam. The calculation parameters used for this analysis are $\Omega = 0.1\,\mathrm{m}^{-1}$,
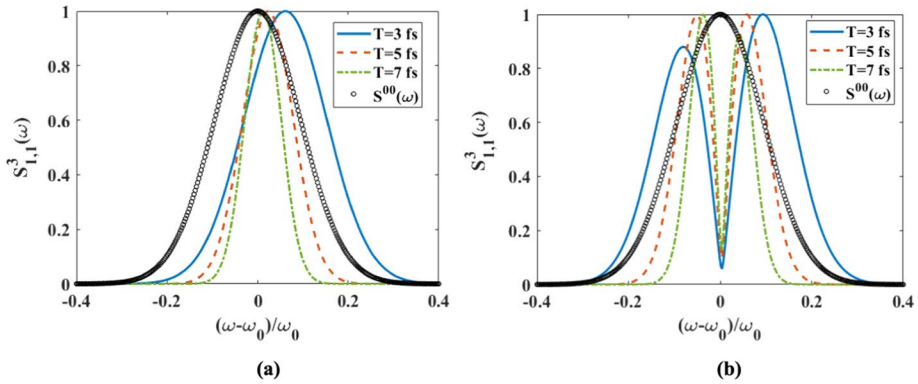
Fig. 3 Normalized spectral intensity of pulsed LHChG beam in oceanic turbulence with varying pulse duration, for both **a** on-axis and **b** off-axis ($\rho_x = 0.2286$ m)
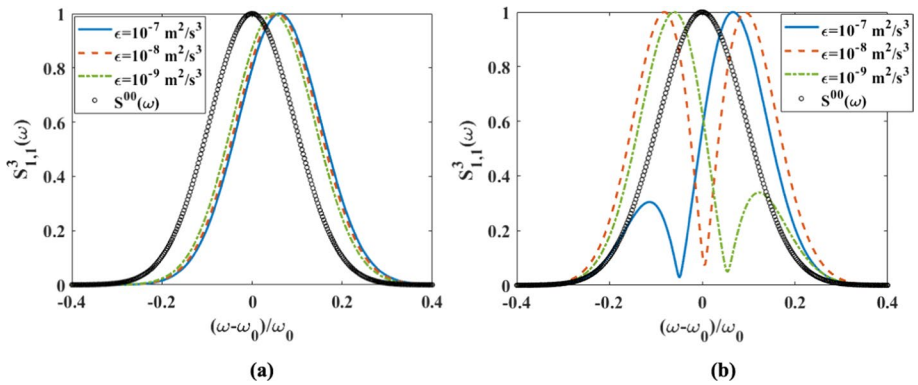
Fig. 4 Normalized spectral intensity of pulsed LHChG beam in oceanic turbulence with varying the rate of dissipation of kinetic energy per unit mass of fluid, for both **a** on-axis and **b** off-axis ($\rho_x = 0.24$ m)

$\varepsilon = 10^{-7}$ m^2/s^3, $\chi_t = 10^{-3}$ K^2/s, $\varpi = -3$, $\lambda = 532$ nm, $w_{0x} = w_{0y} = 1$ mm, $z = 900$ m, $\omega_0 = 2\pi c/\lambda$, $T = 3fs$, $\rho_y = 0$, m $= l = 1$ and $n = 3$.

We depict in Fig. 3, the normalized on-axis and off-axis spectral intensities of the pulsed LHChG beam for different values of the pulse duration. The original spectral intensity is indicated by circles. As depicted in Fig. 3a, it's clear that the on-axis spectral intensity of the pulsed LHChG beam shows a blue-shift, which decreases as the pulse duration increases. However, Fig. 3b displays the normalized off-axis ($\rho_x = 0.2286$ m) spectral intensity of the pulsed LHChG beam. The results show that the spectral intensity has a blue-shift and is divided into two peaks with different heights. At T $= 3$ fs, the initially blue-shifted spectrum splits into two peaks with unequal heights. As the pulse duration increases, the blue shift decreases, and the two peaks become equal in height at T $= 5$ fs. Beyond T $= 7$ fs, the secondary peak becomes higher than the first.

Figure 4 displays the normalized on-axis and off-axis spectral intensity of the pulsed LHChG beam for various values of the rate of dissipation of kinetic energy per unit mass

of fluid. The original spectral intensity is depicted as circles. In Fig. 4a, it is evident that the on-axis spectral intensity of the pulsed LHChG beam has a blue shift. Moreover, the magnitude of this blue shift increases as ε increases. In contrast, Fig. 4b illustrates that the off-axis spectral intensity of the pulsed LHChG beam has a blue shift and is split into two peaks with different heights. As ε decreases, the second peak increases gradually in height. At $\varepsilon = 10^{-8} \mathrm{m}^2/\mathrm{s}^3$ the spectrum is split into two peaks with equal heights. This phenomenon is called the spectral switch. Further decreasing ε to $\varepsilon = 10^{-9} \mathrm{m}^2/\mathrm{s}^3$ leads to the second peak becoming the maximum peak, i.e., the spectrum is red-shifted.

The normalized on-axis and off-axis spectral intensities of the pulsed LHChG beam for different values of the dissipation rate of temperature variance χ_t are depicted in Fig. 5, respectively, where the circles denote the normalized original spectrum. Figure 5a shows that the normalized on-axis spectrum is blue-shifted, and the blue shift increases with increasing χ_t. For example, for $\chi_t = 10^{-6} \mathrm{K}^2/\mathrm{s}$, $\chi_t = 10^{-5} \mathrm{K}^2/\mathrm{s}$, and $\chi_t = 10^{-3} \mathrm{K}^2/\mathrm{s}$, we have $\delta\omega/\omega_0 = 0.0334, 0.0522$ and 0.0602, respectively. However, as illustrated in Fig. 5b, the off-axis ($\rho_x = 0.12\,\mathrm{m}$) spectral intensity exhibits a red shift, which becomes a blue shift with an increase in the dissipation rate of temperature variance χ_t. For instance, for values of $\chi_t =: 10^{-6} \mathrm{K}^2/\mathrm{s}$, $10^{-5} \mathrm{K}^2/\mathrm{s}$ and $10^{-3} \mathrm{K}^2/\mathrm{s}$, the corresponding spectral shifts are $\delta\omega/\omega_0 = -0.0147, 0.0067$, and 0.0682, respectively.
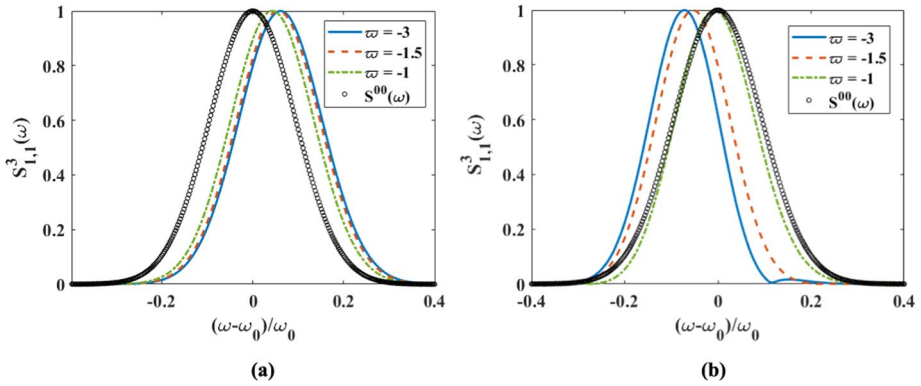
Figure 6 shows the normalized on-axis and off-axis spectral intensities of the pulsed LHChG beam for different values of the ratio of the temperature and salinity contributions to the refractive index spectrum, indicated by ϖ. The original normalized spectrum is represented by circles. In Fig. 6a, it is evident that the spectral intensity along the axis of the pulsed LHChG beam is blue-shifted, and that its magnitude of this blue shift decreases as ϖ increases.

Conversely, the off-axis spectral intensity is red-shifted for all values of ϖ (from the results in Fig. 6b), and the red shift increases as ϖ decreases. These observations suggest that the on-axis and off-axis spectra tend to approach the original spectrum when is close to $\varpi = -1$.

Figure 7 depicts the off-axis relative spectral shift of a pulsed LHChG beam in oceanic turbulence as a function of transverse coordinate ρ_x for various pulse durations and different values of the ratio of temperature and salinity contributions to the refractive index spectrum ϖ. Within the range of 0 to 0.5 m, the spectrum shows a slight blue
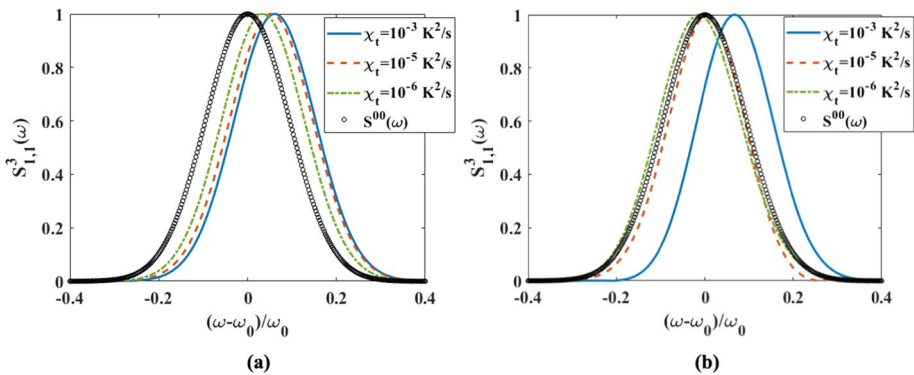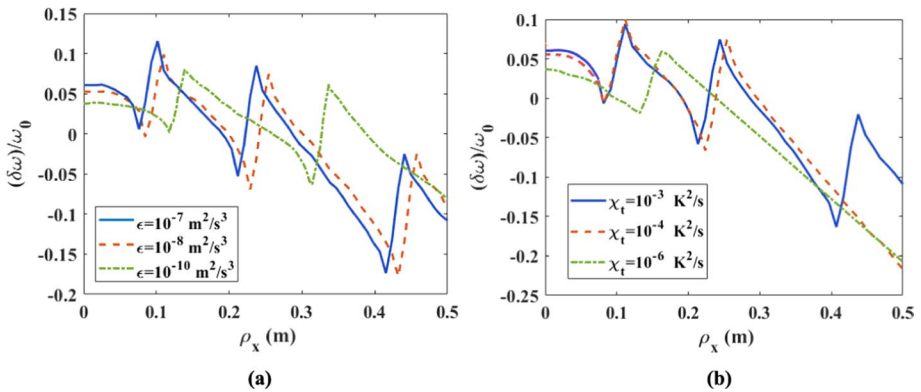

Fig. 5 Normalized spectral intensity of pulsed LHChG beam in oceanic turbulence for three values of the dissipation rate of temperature variance with **a** on-axis and **b** off axis ($\rho_x = 0.12$ m)
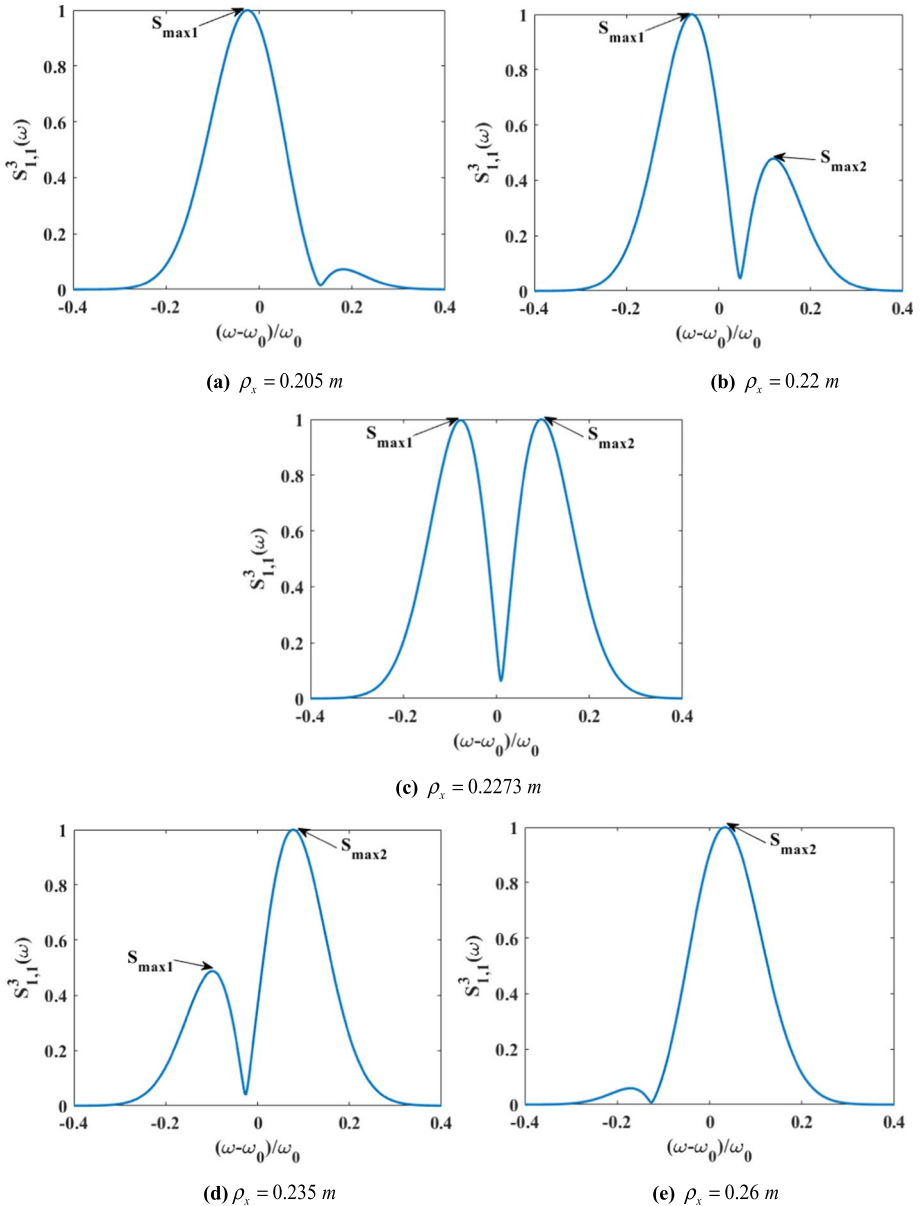
Fig. 6 Normalized spectral intensity of pulsed LHChG beam in oceanic turbulence for three values of the ratio of temperature and salinity contributions to the refractive index spectrum with **a** on-axis and **b** off axis ($\rho_x = 0.35$ m)
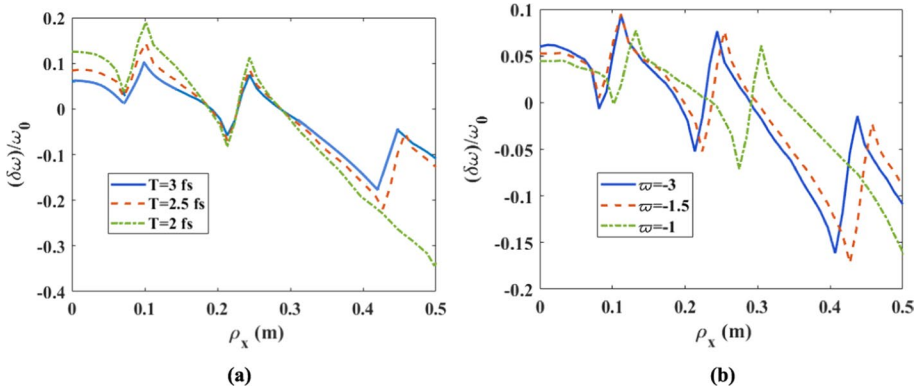
Fig. 7 Relative spectral shift versus ρ_x for the different **a** pulse duration and **b** the ratio of temperature and salinity contributions to the refractive index spectrum

Fig. 8 Relative spectral shift versus ρ_x and for the different **a** the rate of dissipation of kinetic energy per unit mass of fluid and **b** the dissipation rate of temperature variance

Fig. 9 The variation of normalized off-axis spectral intensity of pulsed LHChG beam in oceanic turbulence

shift at the starting point of $\rho_x = 0$, and this blue shift becomes more pronounced as both the pulse duration decreases and increases. As the transverse coordinate continues to increase, the spectrum exhibits a red shift, and the magnitude of this red shift gradually increases, accompanied by a spectral switch.

Additionally, it can be observed that the third spectral switch disappears as T decreases (see Fig. 7a) and ϖ increases (see Fig. 7b).

In Fig. 8, the off-axis relative spectral shift is shown as a function of the transverse coordinate ρ_x for different values of the rate of dissipation of kinetic energy per unit mass of fluid ε and the dissipation rate of temperature variance χ_t. This figure shows that the spectral shift exhibits a slight blue shift at $\rho_x = 0$, and the blue shift becomes larger as ε and χ_t increase. As the position parameter continues to increase, the spectrum is red-shifted, and the amount of red shift increases gradually, accompanied by a spectral switch.

Figure 8a demonstrates that with the decrease of the energy dissipation rate per unit mass ε, the third spectral switches disappears for the case of $\varepsilon = 10^{-10}\, \mathrm{m}^2/\mathrm{s}^3$. On the other hand, Fig. 8b shows that with decreasing the dissipation rate of temperature variance χ_t and as the position parameter increases, the third spectral switch disappears for the case of $\chi_t = 10^{-4}\, \mathrm{K}^2/\mathrm{s}$. In addition, the second and third spectral switches disappear for the case of $\chi_t = 10^{-6}\, \mathrm{K}^2/\mathrm{s}$.

In Fig. 9, the normalized off-axis spectral intensity of a pulsed LHChG beam propagating through the oceanic turbulence for different values of the transverse coordinate is depicted.

It is shown that the off-axis spectrum is split into two peaks, i.e., one maximum peak with the second peak. Figures 9a and b show that as ρ_x increases from 0.205 to 0.22 m, the red shift increases and the second peak of the spectrum becomes large. Figure 9c shows that the two peaks reach the same height at $\rho_x = 0.2273$ m. Figures 9d and e show that as d continues to increase, blue shift occurs and the blue shift decreases gradually. This means that the spectral shift changes abruptly from red to blue when ρ_x reaches a critical value.

4 Conclusion

In summary, the changes in spectral intensity of a pulsed LHChG beam as it propagates through oceanic turbulence are investigated in the present work. To achieve that, a formula based on the Huygens-Fresnel principle and Fourier Transform method is presented, and numerical simulations are conducted to validate the results. The paper analyzes the impact of oceanic turbulence parameters and pulse duration on the spectral behavior of the beam and provides a physical explanation for the spectral transition observed. The findings have significant implications for information coding and transmission.

Data availability No datasets is used in the present study.

Declarations

Conflict of interest The authors have no financial or proprietary interests in any material discussed in this article.

Consent for publication The authors confirm that there is informed consent to the publication of the data contained in the article.

References

Abramowitz, M., Stegun, I.: Handbook of mathematical functions with formulas, graphs, and mathematical tables. US Department of Commerce, Washington DC (1970)

Agrawal, G.P.: Far-field diffraction of pulsed optical beams in dispersive media. Opt. Commun. **167**, 15–22 (1999)

Andrews, L.C., Phillips, R.L.: Laser beam propagation through random media. SPIE Press, Bellingham (2005)

Belafhal, A., Hricha, Z., Dalil-Essakali, L., Usman, T.: A note on some integrals involving Hermite polynomials and their applications. Adv. Math. Mod. Appl. **5**, 313–319 (2020)

Belafhal, A., Chib, S., Khannous, F., Usman, T.: Evaluation of integral transforms using special functions with applications to biological tissues. Comput. Appl. Math. **40**, 156–178 (2021)

Benzehoua, H., Dalil-Essakali, L., Belafhal, A.: Analysis of the modulation depth of femtosecond dark hollow laser pulses. Quant. Electron. **53**, 1–18 (2021a)

Benzehoua, H., Dalil-Essakali, L., Belafhal, A.: Production of good quality holograms by the THz pulsed vortex beams. Quant. Electron. **54**, 1–13 (2021b)

Boufalah, F., Dalil-Essakali, L., Ez-Zariy, L., Belafhal, A.: Introduction of generalized Bessel–Laguerre–Gaussian beams and its central intensity travelling a turbulent atmosphere. Opt. Quant. Electron. **50**, 305–320 (2018)

Boufalah, F., Dalil-Essakali, L., Belafhal, A.: Scintillation index analysis of generalized Bessel-Laguerre-Gaussian beam. Opt. Quant. Electron. **54**(10), 616 (2022)

Chang, S., Song, Y., Dong, Y., Dong, K.: Spreading properties of a multiGaussian Schell-model vortex beam in slanted atmospheric turbulence. Opt. Appl. **50**, 83–94 (2020)

Chib, S., Dalil-Essakali, L., Belafhal, A.: Evolution of the partially coherent Generalized Flattened Hermite–Cosh–Gaussian beam through a turbulent atmosphere. Opt Quant Electron **52**, 484–500 (2020)

Duan, M., Tian, Y., Zhang, Y., Li, J.: Influence of biological tissue and spatial correlation on spectral changes of Gaussian-Schell model vortex beam. Opt. Lasers Eng. **134**, 106224–106230 (2020)

Han, P.: Lattice spectroscopy. Opt. Lett. **34**, 1303–1305 (2009)

Hricha, Z., Lazrek, M., Yaalou, M., Belafhal, A.: Propagation of vortex cosine-hyperbolic-Gaussian beams in atmospheric turbulence. Opt. Quant. Electron. **53**, 383–398 (2021)

Jo, J.H., Ri, O.H., Ju, T.Y., Pak, K.M., Ri, S.G., Hong, K.C., Jang, S.H.: Effect of oceanic turbulence on the spectral changes of diffracted chirped Gaussian pulsed beam. Opt. Laser Technol. **153**, 108200–108208 (2022)

Johnson, L.J., Green, R.J., Leeson, M.S.: Underwater optical wireless communications: depth-dependent beam refraction. Appl. Opt. **53**, 7273–7277 (2014)

Kandpal, H.C., Vaishya, J.S.: Experimental observation of the phenomenon of spectral switching for a class of partially coherent light. IEEE J. Quant. Electron. **38**, 336–339 (2002)

Korotkova, O., Farwell, N., Shchepakina, E.: Light scintillation in oceanic turbulence. Waves in Random Complex Med. **22**, 260–266 (2012)

Li, Y., Zhang, Y.X., Zhu, Y.: Oceanic spectrum of unstable stratification turbulence with outer scale and scintillation index of Gaussian beam wave. Opt. Express **27**, 7656–7672 (2019)

Li, Y., Zhang, Y., Zhu, Y.: Lommel–Gaussian pulsed beams carrying orbital angular momentum propagation in asymmetric oceanic turbulence. IEEE Photon. J. **12**, 7900915–7900930 (2020)

Liu, D., Lü, B.: Spectral shifts and spectral switches in diffraction of ultrashort pulsed beams passing through a circular aperture. Optik **115**, 447–454 (2004)

Liu, D., Wang, Y.: Evolution properties of a radial phased-locked partially coherent Lorentz–Gauss array beam in oceanic turbulence. Opt. Laser Technol. **103**, 33–41 (2018)

Liu, D., Wang, Y., Wang, G., Yin, H., Wang, J.: The influence of oceanic turbulence on the spectral properties of chirped Gaussian pulsed beam. Opt. Laser Technol. **82**, 76–81 (2016)

Nossir, N., Dalil-Essakali, L., Belafhal, A.: Behavior of the central intensity of generalized humbert-gauss-ian beams against the atmospheric turbulence. Opt. Quant. Electron. **53**, 665–677 (2021)

Wu, Y., Zhang, Y., Li, Y., Hu, Z.: Beam wander of Gaussian–Schell model beams propagating through oce-anic turbulence. Opt. Commun. **371**, 59–66 (2016)

Xu, J., Zhao, D.: Propagation of a stochastic electromagnetic vortex beam in the oceanic turbulence. Opt. Laser Technol. **57**, 189–193 (2014)

Yadav, B.K., Rizvi, S.A.M., Raman, S., Mehrotra, R., Kandpal, H.C.: Information encoding by spectral anomalies of spatially coherent light diffracted by an annular aperture. Opt. Commun. **269**, 253–260 (2007)

Yadav, B.K., Raman, S., Kandpal, H.C.: Information exchange in free spacing using spectral switching of diffracted polychromatic light: possibilities and limitations. J. Opt. Soc. Am. A **25**, 2952–2959 (2008)

Zhu, B.Y., Bian, S.J., Tong, Y., Mou, X.Y., Cheng, K.: Spectral properties of partially coherent chirped Airy pulsed beam in oceanic turbulence. Optoelectron. Lett. **17**, 123–128 (2021)

Zou, Q., Hu, Q.: Spectral anomalies of diffracted chirped pulsed super-Gaussian beam. Optik **127**, 1967–1971 (2016)